

## Psychophysical discrimination of radially varying polarization-based entoptic phenomena

D.A. Pushin,<sup>1,2,3,\*</sup> C. Kapahi<sup>1,2</sup> A.E. Silva<sup>4</sup>, D.G. Cory,<sup>1,5</sup> M. Kulmaganbetov<sup>2,3</sup>,  
M. Mungalsingh<sup>4</sup>, T. Singh<sup>3</sup>, B. Thompson<sup>3,4</sup> and D. Sarenac<sup>1,3,6,†</sup>

<sup>1</sup>*Institute for Quantum Computing, University of Waterloo, Waterloo, Ontario N2L 3G1, Canada*

<sup>2</sup>*Department of Physics, University of Waterloo, Waterloo, Ontario N2L 3G1, Canada*

<sup>3</sup>*Centre for Eye and Vision Research, 17W Hong Kong Science Park, Hong Kong, China*

<sup>4</sup>*School of Optometry and Vision Science, University of Waterloo, Waterloo, Ontario N2L 3G1, Canada*

<sup>5</sup>*Department of Chemistry, University of Waterloo, Waterloo, Ontario N2L 3G1, Canada*

<sup>6</sup>*Department of Physics, University at Buffalo, State University of New York, Buffalo, New York 14260, USA*

(Received 15 June 2023; revised 9 December 2023; accepted 19 December 2023; published 24 January 2024)

The incorporation of structured-light techniques into vision science has enabled more-selective probes of polarization-related entoptic phenomena. Diverse sets of stimuli have become accessible in which the spatially dependent optical properties can be rapidly controlled and manipulated. For example, past studies in human perception of polarization have dealt with stimuli that appear to vary azimuthally. This is mainly due to the constraint that the typically available degree of freedom to manipulate the phase shift of light rotates the perceived pattern around a person's point of fixation. Here we create a structured-light stimulus that is perceived to vary purely along the radial direction and test discrimination sensitivity to inward and outward radial motion. This is accomplished by our preparing a radial state coupled to an orbital-angular-momentum state that matches the orientation of the dichroic elements in the macula. By expanding the range of entoptic images induced by structured light, this method will accelerate the development of structured-light tools for the assessment and monitoring of macular health.

DOI: 10.1103/PhysRevApplied.21.L011002

**Introduction.** The preparation, manipulation, and characterization of structured light [1–4] have yielded impactful advances across a wide range of fields, including applications in high-resolution imaging, optical metrology, high-bandwidth communication, and material characterization [5–16]. The backbone of structured-light techniques is the tailoring of optical wave fronts and the inducing of coupling between different degrees of freedom to obtain nontrivial propagation characteristics such as orbital angular momentum (OAM), nondiffraction, and self-acceleration. Recent work has applied the structured-light toolbox to the vision sciences [17–20], increasing the ability to explore entoptic phenomena through the use of polarization-coupled OAM states. Whereas uniformly polarized light induces the perception of a “Haidinger brush” that is a bow-tie-like shape with two azimuthal fringes [21], the structured light beams were shown to be capable of inducing a large and varying number of entoptic azimuthal fringes [17]. A follow-up study showed

that the visual angle of the polarization-related entoptic phenomena increases for a higher number of fringes [20].

The human perception of polarization states of light is enabled by a series of radially symmetric dichroic elements (macular pigment) centered at the foveola in the human eye [22–25]. The spatial orientation of the radially oriented axonal fibers of retinal cells (mainly ganglion cells and photoreceptors) coupled with macular pigment effectively forms a weak radial polarizer within the retinal microstructure [26,27]. This feature has been exploited by polarized-light studies of central-visual-field dysfunction and age-related macular degeneration [28,29], macular-pigment-density profiles [30], and the location of the fovea [31]. Early detection of age-related macular degeneration is of particular importance as age-related macular degeneration is a major cause of blindness worldwide [32].

Here we explore the use of structured light that induces the perception of fringes purely varying along the radial direction relative to the central point of vision. This is accomplished through the use of structured light that possesses a coupling between radial states and the  $l = 2$  orbital state that matches the symmetry of the dichroic macular pigment. The net result is the perception of entoptic

\*dmitry.pushin@uwaterloo.ca

†dusansar@buffalo.edu

radial fringes that move inward or outward relative to the center point. The macular-pigment profile is azimuthally symmetric, sharply peaking at the center point of vision. Therefore, azimuthally varying entoptic motion is along the direction of constant macular-pigment density, while radially varying entoptic motion is along the direction with the most change in macular-pigment density. The method presented offers a new dimension of exploration of entoptic phenomena and serves as a complement to the previous studies that used azimuthally varying fringes. Harnessing multiple modalities of structured light to reveal the radial-polarization properties of the human eye may enable new approaches to the early detection of diseases that alter macular structure such as age-related macular degeneration.

*Methods.* The setup used in this study is described in detail in Ref. [20]. Here we give a basic overview. The setup uses a spatial light modulator (SLM) to induce an arbitrary phase profile on the incoming beam. The pixel size of the SLM, and hence the available resolution, is 3  $\mu\text{m}$ . A 4f imaging system in combination with a 20D Volk lens projects the profile from the SLM onto the participant's retina. This microscopy-inspired method ensures that free-space propagation effects do not occur and alter the stimuli. If, on the other hand, the beam were allowed to freely propagate until it reached the eye, the doughnutlike diffraction from the OAM states and the ringlike diffraction from the

circular obstruction would significantly alter the perceived entoptic profile. A small aperture illuminated by red light is present in the middle of the stimulus to serve as a fixation point.

The target transverse wave function of the structured light beams for this study can be written as

$$|\Psi\rangle = \frac{1}{\sqrt{2}}(1 - \Pi[r/c]) [e^{i(n_r r + \ell\phi + \theta t)} |R\rangle + |L\rangle], \quad (1)$$

where  $(r, \phi)$  are the transverse coordinates,  $n_r$  and  $\ell$  are the radial and OAM numbers,  $|L\rangle$  and  $|R\rangle$  are the right-circularly-polarized and left-circularly-polarized states,  $\Pi[r/c]$  is the unit pulse function that sets the size ( $c$ ) of the central obstruction area, and  $\theta t$  is a time-varying phase shift that dictates the speed of the perceived radial motion. A speed  $\theta = 1800^\circ/\text{s}$  was chosen in this study as this corresponds to a temporal frequency of 5 Hz at any spatial location, which allows sufficient motion within a total presentation of 500 ms. The OAM value  $\ell = 2$  was chosen so as to match the symmetry of the dichroic macular-pigment elements and induce a radial varying stimulus. The radial number  $n_r = 2\pi/p_r$  sets the period ( $p_r$ ) of the radial gradients, and a radial period  $p_r = 20$  pixels on the SLM was chosen as it roughly corresponds to  $p_r = 0.9^\circ$  of the visual field. The spatially dependent phase and polarization profile of this state is depicted in Fig. 1(a).

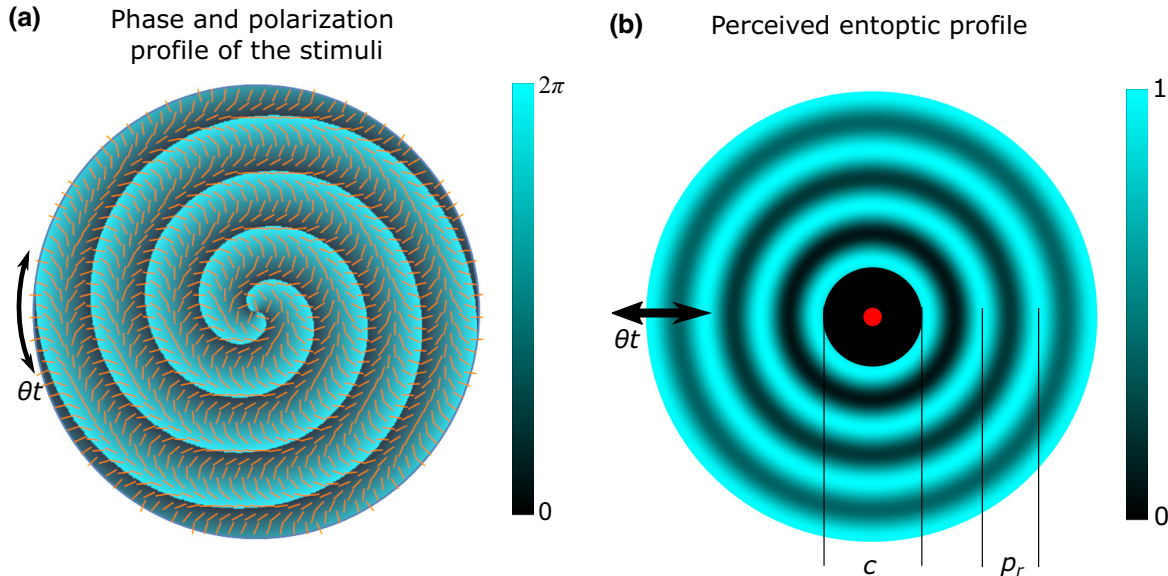


FIG. 1. (a) The spatially dependent polarization (yellow bars) and phase (blue-black color map) profile of the stimuli used in the study. (b) Simulated entoptic pattern that would be perceived by a participant with a healthy macula. Although the contrast of the extent of the visible area may vary from participant to participant, a participant with normal vision will perceive a series of concentric circles. The eye's radial filter perceptually removes the spiral feature, and the final percept is that of radial waves. A radial blur is applied to depict the effect of decreasing macular-pigment density along the radial direction. The clockwise or counterclockwise rotation of the beam in (a) results in an inward or outward motion of the perceived radial pattern. The experimental stimulus included a central red-light fixation guide, as shown. Finally, the size of the centrally blocked region, depicted in black, was varied to control the difficulty of the task and to measure the peripheral extent of sensitivity to radial entoptic motion.

The entoptic profile that a participant will observe can be approximated by determination of the intensity after light whose wave function is described by Eq. (1) passes through a radial-polarization filter:

$$I = (1 - \Pi[r/c]) \cos^2 \left( \frac{1}{2} (2\pi r/p_r + \theta t) \right), \quad (2)$$

which is depicted in Fig. 1(b). Figure 1(b) also shows the red-light fixation point and the expected radial blur that occurs with decreasing macular-pigment density along the radial direction.

Eighteen participants were recruited to perform a motion-direction-discrimination task. All participants provided informed consent and were treated in accordance with the Declaration of Helsinki. All research procedures received approval from the University of Waterloo Office of Research Ethics. Before the main task, all participants performed a familiarization task in which an obstruction with a size of 20 pixels was presented ten times. During these presentations, the stimulus duration was self-timed so that participants could learn to perform the task—most participants answered within a 2–5-s presentation window. All participants achieved at least 70% discrimination accuracy in the familiarization task.

Participants discriminated the radial motion of the entoptic pattern, appearing to move either inward or outward. The obstruction region ( $c$ ) on the SLM was varied according to a two-up, one-down psychophysical staircase.

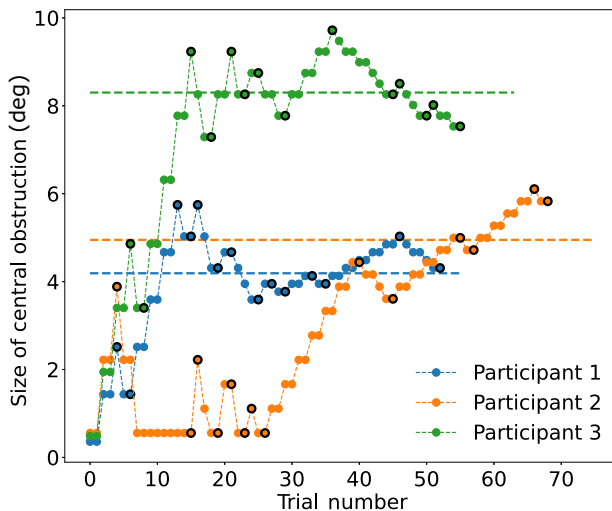


FIG. 2. The psychophysical study used a staircase method where the size of the obstruction was varied according to the accuracy of the participant’s responses. Shown are data for three different participants, with reversal points highlighted with a black outline. Threshold values from this two-up, one-down staircase, computed from the final six reversal points, are shown as dotted horizontal lines. The thresholds are converted into visual-angle units through retinal imaging with the structured-light stimulus, as described in Ref. [20].

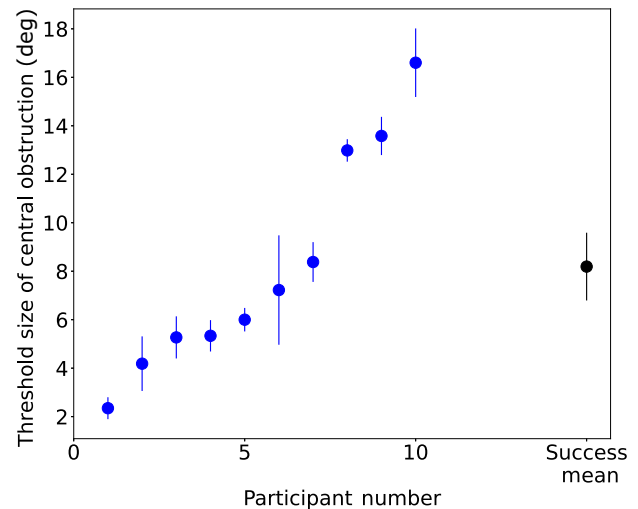


FIG. 3. Threshold values, plotted in ascending order, for each participant. The measured mean was  $8.2^\circ \pm 1.4^\circ$  (standard deviation  $6.4^\circ$ ) with a 95% confidence interval of  $3.8^\circ$ – $12.6^\circ$ . It was found that it was noticeably harder for a participant to perceive radial entoptic motion than azimuthally varying motion. Seven of the 18 participants exhibited three reversals at the performance floor, indicating poor performance. Furthermore, the mean threshold size indicates that at a comparable eccentricity, roughly 3 times as much entoptic oscillation density was required to detect radial entoptic motion (this task) compared with azimuthal motion in Ref. [20].

The obstruction region became larger after two consecutive correct responses and became smaller after every incorrect response. This procedure resulted in an obstruction size threshold indicating the eccentric extent of sufficient polarization sensitivity to achieve at least 70.7% performance accuracy. A larger threshold indicates a larger eccentric range of polarization sensitivity.

A “reversal” was counted when the obstruction region had been enlarged in previous trials but became smaller in a subsequent trial or vice versa. The task was completed after 14 reversals or after 90 total stimulus presentations. The arithmetic mean of the final six reversals was taken as the performance threshold. If the participant completed 90 stimulus presentations, then the final point was counted as a reversal. The initial obstruction size had a radius of 10 pixels and obstructed nothing beyond what the red fixation light obstructed. The obstruction radius was updated by 30 pixels after the first three reversals, by 20 pixels after the following three reversals, by 10 pixels after another three reversals, and finally by 5 pixels for the remaining reversals. Three examples of staircases with corresponding thresholds are shown in Fig. 2.

In the last step of the study, two retinal images were taken, the first with a standard fundus imaging system and the second with the structured-light imaging system, allowing the psychophysically defined threshold to be converted into degrees of visual angle [20].

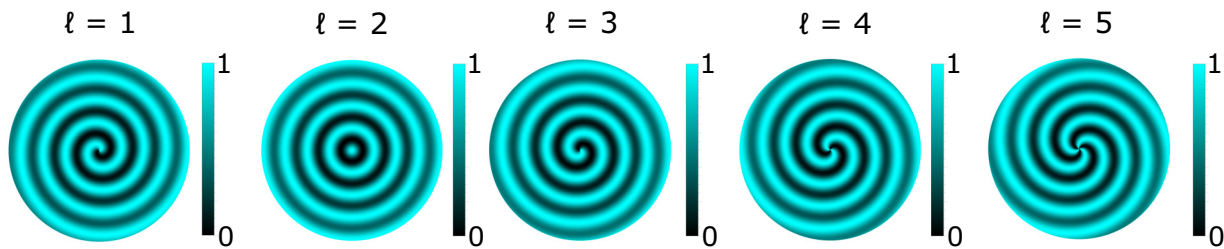


FIG. 4. Entoptic patterns that arise from the perception of stimuli composed of a radial state that is coupled to various OAM states. As shown, the OAM  $\ell \neq 2$  cases can induce spiral-like entoptic profiles where the magnitude of the OAM value determines the number of spiral arms, the sign of the OAM value determines the spiral handedness, and the magnitude of the radial value determines the strength of the spiral winding. The entoptic motion that is varied with a polarization-dependent phase shift would therefore possess both an azimuthal component and a radial component, providing rich avenues of exploration.

*Study results and discussion.* Subjective reports from the participants and authors verify that observers perceive the stimulus as a series of concentric circles that radiate inward or outward from the central fixation point. The average obstruction size threshold (in degrees of visual angle) for the ten participants with successful staircase convergence was  $8.2^\circ \pm 1.4^\circ$  (standard deviation  $6.4^\circ$ ) with a 95% confidence interval of  $3.8^\circ$ – $12.6^\circ$ . This demonstrates that while polarization sensitivity differed between observers, it could be reliably measured even  $4^\circ$  away from fixation. See Fig. 3 for participant-by-participant and summary results.

Staircases that contain more than three reversal points at the minimum central obstruction are considered “failed” and without sufficient sensitivity to measure a reliable threshold. It was found that most participants had relatively more difficulty in reliably perceiving the radial motion than the azimuthal motion, and seven participants failed the task. Furthermore, one outlier participant, as defined by a threshold 3 standard deviations from the group mean, was excluded from analysis on the assumption of confounding eye movements. A possible cause of the relative difficulty could be that in comparison with azimuthally varying stimuli, where the fringe oscillations are along the direction of constant macular-pigment density, radially varying entoptic motion is along the direction with the most change in macular-pigment density. Another possible cause could be that the feature size of the azimuthally varying stimuli naturally scales for eccentricity, potentially compensating for decreased visual acuity outside of central fixation.

To compare the perception sensitivity of azimuthal and radial stimuli, we can consider the relative size on the retina that one oscillation period occupies in each case. For entoptic motion that is a distance of  $c/2$  away from the central point of fixation, the oscillation period is  $\pi c/N$  for azimuthal stimuli while for radial stimuli the oscillation period is equal to  $p_r$  and it is independent of  $c$ . Connor *et al.* [20] considered a stimulus with  $N = 11$  azimuthal oscillations and reported an average central obstruction threshold  $c$  of approximately  $9.5^\circ$ , which corresponds to an azimuthal oscillation period of approximately  $2.7^\circ$  near

the obstruction edge, whereas the stimuli in this work possessed a 3 times smaller radial oscillation period  $p_r$  of approximately  $0.9^\circ$  and we reported a comparable average central obstruction threshold of  $8.2^\circ$ . The variability of thresholds reported here and in Ref. [20] demonstrates the range of responses expected from a healthy population. Similarly to other psychophysical tasks, overall performance may also be affected by factors such as fixation stability, comfort and fatigue, and familiarity with entoptic phenomena. However, this task is particularly useful as a probe of the visual processing of a stimulus that is directly dependent on the macular pigment, potentially capturing a unique radial dimension of pigment density that has otherwise never been reported with other entoptic stimuli.

*Conclusion.* The techniques described here can provide a complementary set of data when one is analyzing a person’s ability to perceive entoptic stimuli. The addition of this radial dimension of testing will allow us to perform more-accurate characterization and reconstruction of an individual’s macular structure that is responsible for the perception of polarization-related entoptic phenomena. These objective measures may allow greater power to characterize normal and abnormal limits to the extent of the macula sensitive to polarization-defined entoptic stimuli, ultimately probing the health of the underlying macular pigment, which directly supports performance in this task.

Future studies will use stimuli with radial states coupled to various OAM states. As shown in Fig. 4, the corresponding entoptic profiles can take on a spiral-like shape where the magnitude of the OAM value determines the number of spiral arms and the magnitude of the radial value determines the strength of the spiral winding. We expect this to be a rich avenue of exploration as the entoptic motion that is varied with a polarization-dependent phase shift would possess both an azimuthal component and a radial component.

*Acknowledgments.* This work was supported by the Canadian Excellence Research Chairs program, the Natural Sciences and Engineering Research Council of Canada

(Grants No. RGPIN-2018-04989, No. RPIN-05394, and No. RGPAS-477166), the Government of Canada's New Frontiers in Research Fund (Grant No. NFRFE-2019-00446), the Velux Stiftung Foundation (Grant No. 118), the InnoHK initiative and the Hong Kong Special Administrative Region Government, and the Canada First Research Excellence Fund. D.A.P. is grateful to Sonja Franke-Arnold for fruitful discussions.

- [1] Halina Rubinsztein-Dunlop, Andrew Forbes, M. V. Berry, M. R. Dennis, David L. Andrews, Masud Mansuripur, Cornelia Denz, Christina Alpmann, Peter Banzer, and Thomas Bauer *et al.*, Roadmap on structured light, *J. Opt.* **19**, 013001 (2016).
- [2] K. Y. Bliokh, E Karimi, M. J. Padgett, M. A. Alonso, M. R. Dennis, A Dudley, A Forbes, S Zahedpour, S. W. Hancock, and H. M. Milchberg *et al.*, Roadmap on structured waves, *J. Opt.* **25**, 103001 (2023).
- [3] Jian Chen, Chenhao Wan, and Qiwen Zhan, Engineering photonic angular momentum with structured light: A review, *Adv. Photonics* **3**, 064001 (2021).
- [4] Jincheng Ni, Can Huang, Lei-Ming Zhou, Min Gu, Qinghai Song, Yuri Kivshar, and Cheng-Wei Qiu, Multidimensional phase singularities in nanophotonics, *Science* **374**, eabj0039 (2021).
- [5] Alois Mair, Alipasha Vaziri, Gregor Weihs, and Anton Zeilinger, Entanglement of the orbital angular momentum states of photons, *Nature* **412**, 313 (2001).
- [6] M. F. Andersen, C. Ryu, P. Cladé, V. Natarajan, A. Vaziri, K. Helmerson, and W. D. Phillips, Quantized rotation of atoms from photons with orbital angular momentum, *Phys. Rev. Lett.* **97**, 170406 (2006).
- [7] Sacha Schwarz, Connor Kapahi, Ruoxuan Xu, Andrew R. Cameron, Dusan Sarenac, Jean-Philippe W. MacLean, Katanya B. Kuntz, David G. Cory, Thomas Jennewein, Kevin J. Resch, and D. A. Pushin, Talbot effect of orbital angular momentum lattices with single photons, *Phys. Rev. A* **101**, 043815 (2020).
- [8] Monika Ritsch-Marte, Orbital angular momentum light in microscopy, *Philos. Trans. R. Soc., A: Mathematical, Physical and Engineering Sciences* **375**, 20150437 (2017).
- [9] Jian Wang, Jeng-Yuan Yang, Irfan M. Fazal, Nisar Ahmed, Yan Yan, Hao Huang, Yongxiong Ren, Yang Yue, Samuel Dolinar, Moshe Tur, and Alan E. Willner, Terabit free-space data transmission employing orbital angular momentum multiplexing, *Nat. Photonics* **6**, 488 (2012).
- [10] Miles Padgett and Richard Bowman, Tweezers with a twist, *Nat. Photonics* **5**, 343 (2011).
- [11] Christian Maurer, Alexander Jesacher, Severin Fürhapter, Stefan Bernet, and Monika Ritsch-Marte, Tailoring of arbitrary optical vector beams, *New J. Phys.* **9**, 78 (2007).
- [12] L. Marrucci, C. Manzo, and D. Paparo, Optical spin-to-orbital angular momentum conversion in inhomogeneous anisotropic media, *Phys. Rev. Lett.* **96**, 163905 (2006).
- [13] D. Sarenac, D. G. Cory, J. Nsofimi, I. Hincks, P. Miguel, M. Arif, Charles W. Clark, M. G. Huber, and D. A. Pushin, Generation of a lattice of spin-orbit beams via coherent averaging, *Phys. Rev. Lett.* **121**, 183602 (2018).
- [14] Giovanni Milione, Martin P. J. Lavery, Hao Huang, Yongxiong Ren, Guodong Xie, Thien An Nguyen, Ebrahim Karimi, Lorenzo Marrucci, Daniel A. Nolan, Robert R. Alfano, and Alan E. Willner,  $4 \times 20$  Gbit/s mode division multiplexing over free space using vector modes and a  $q$ -plate mode (de)multiplexer, *Opt. Lett.* **40**, 1980 (2015).
- [15] Andrew R. Cameron, Sandra W. L. Cheng, Sacha Schwarz, Connor Kapahi, Dusan Sarenac, Michael Graboweczyk, David G. Cory, Thomas Jennewein, Dmitry A. Pushin, and Kevin J. Resch, Remote state preparation of single-photon orbital-angular-momentum lattices, *Phys. Rev. A* **104**, L051701 (2021).
- [16] Lorenzo Marrucci, Ebrahim Karimi, Sergei Slussarenko, Bruno Piccirillo, Enrico Santamato, Eleonora Nagali, and Fabio Sciarrino, Spin-to-orbital conversion of the angular momentum of light and its classical and quantum applications, *J. Opt.* **13**, 064001 (2011).
- [17] Dusan Sarenac, Connor Kapahi, Andrew E. Silva, David G. Cory, Ivar Tamini, Benjamin Thompson, and Dmitry A. Pushin, Direct discrimination of structured light by humans, *Proc. Natl. Acad. Sci.* **117**, 14682 (2020).
- [18] Dusan Sarenac, Andrew E. Silva, Connor Kapahi, D. G. Cory, B. Thompson, and Dmitry A. Pushin, Human psychophysical discrimination of spatially dependant Pancharatnam-Berry phases in optical spin-orbit states, *Sci. Rep.* **12**, 3245 (2022).
- [19] Lea Gassab, Ali Pedram, and Özgür E. Müstecaplıoğlu, Conditions on detecting three-photon entanglement in psychophysical experiments, arXiv preprint [arXiv:2303.07446](https://arxiv.org/abs/2303.07446) (2023).
- [20] Connor Kapahi, Andrew E. Silva, David G. Cory, Mukhit Kulmaganbetov, Melanie Mungalsingh, Dmitry A. Pushin, Taranjit Singh, Ben Thompson, and Dusan Sarenac, Measuring the visual angle of polarization-related entoptic phenomena using structured light, arXiv preprint [arXiv:2304.12941](https://arxiv.org/abs/2304.12941) (2023).
- [21] Wilhelm Haidinger, Ueber das direkte Erkennen des polarisirten Lichts und der Lage der Polarisationsebene, *Ann. Phys.* **139**, 29 (1844).
- [22] Gary P. Misson, Brenda H. Timmerman, and Peter J. Bryanston-Cross, Human perception of visual stimuli modulated by direction of linear polarization, *Vision Res.* **115**, 48 (2015).
- [23] Gary P. Misson and Stephen J. Anderson, The spectral, spatial and contrast sensitivity of human polarization pattern perception, *Sci. Rep.* **7**, 16571 (2017).
- [24] Gary P. Misson, Shelby E. Temple, and Stephen J. Anderson, Computational simulation of human perception of spatially dependent patterns modulated by degree and angle of linear polarization, *JOSA A* **36**, B65 (2019).
- [25] Qi Wang, Peter J. Bryanston-Cross, Yahong Li, and Zhiying Liu, Mathematical modeling and experimental verification of aging human eyes polarization sensitivity, *JOSA A* **39**, 2398 (2022).
- [26] Gábor Horváth, Gábor Horváth, and Dezsö Varju, *Polarized Light in Animal Vision: Polarization Patterns in Nature* (Springer Science & Business Media, New York City, NY, 2004).

- [27] Jacopo Mottes, Dominga Ortolan, and Gianluca Ruffato, Haidinger's brushes: Psychophysical analysis of an entoptic phenomenon, *Vision Res.* **199**, 108076 (2022).
- [28] H. Walter Forster, The clinical use of the Haidinger's brushes phenomenon, *Am. J. Ophthalmol.* **38**, 661 (1954).
- [29] E. J. Naylor and A. Stanworth, The measurement and clinical significance of the Haidinger effect, *Trans. Ophthal. Soc. U. K.* **75**, 67 (1955).
- [30] Philipp L. Müller, Simone Müller, Martin Gliem, Kristina Küpper, Frank G. Holz, Wolf M. Harmening, and Peter Charbel Issa, Perception of Haidinger brushes in macular disease depends on macular pigment density and visual acuity, *Invest. Ophthalmol. Vis. Sci.* **57**, 1448 (2016).
- [31] Dean A. VanNasdale, Ann E. Elsner, Anke Weber, Masahiro Miura, and Bryan P. Haggerty, Determination of foveal location using scanning laser polarimetry, *J. Vis.* **9**, 21 (2009).
- [32] Laurence S. Lim, Paul Mitchell, Johanna M. Seddon, Frank G. Holz, and Tien Y. Wong, Age-related macular degeneration, *The Lancet* **379**, 1728 (2012).